Generation and Characterization of a Pulsed Dense Plasma with Helium*

T. Manegold, M. Iberler, J. Wiechula and J. Jacoby

Goethe University
Institute of Applied Physics
Frankfurt/Main, Germany

***Abstract*—This contribution is about the characterization of a Lorentz-drift based plasma accelerator in preparation for a colliding plasma experiment. The aim is to investigate the basics of a high energy density collision zone by accelerating two or more plasma sheets simultaneously against each other. Possible applications for this device are UV/VUV backlighting and the production of high densities for plasma stripping. Additionally the device is eligible for basic research of stopping energy. The experimental setup has a total capacitance of 27 µF at maximum voltages of 10 kV. The maximum discharge current of 147 kA is switched by a thyratron. Due to the low total inductance of the setup of 130 nH high current slew rates in the 10^{11} A/s range are achieved. All measurements have been performed in a vacuum chamber at 3 to 100 mbar pressures with a 2% hydrogen in helium gas mixture. For dynamic characterization and optimization of the acceleration process velocity and kinetic energy of the plasma sheet have been investigated. Up to 80 km/s velocities have been determined by a photodiode array and images of a fast framing camera. Moreover the images show the shape of the plasma sheet. Due to the Stark broadening of the H_β-line electron densities in the 10^{15} cm^{-3} range have been determined by a 0.5 m monochromator. The mean temperature has been estimated via He I and He II line intensities. Electron density and temperature of the single accelerator are of great interest for the upcoming comparison to the collision experiment.**

Keywords—plasma sheet; pulsed discharge; Lorentz drift; snowplow model

I. Introduction

Pulsed electromagnetic coaxial plasma accelerators were investigated first in the end of the 1950's by Marshall [1] and Mather [2]. These devices are well known as plasma guns [3], plasma thruster [4] and plasma focus devices [5]. They are of great interest for different fields of application. Worth mentioning here in particular are x-ray lithography [6], plasma refueling for fusion reactors [7], propulsion in space [8] and switching of high currents and voltages [9]. The aim of the presented work is the generation of a high density zone which can possibly be used for ion stripping. Plasma strippers need high electron densities and combine the advantages of efficient stripping foils and durable gas strippers [10]. As an additional application we assume UV/VUV backlighting due to intense He lines in the wavelength range below 164 nm. To generate high electron densities and UV/VUV emission intensities it is necessary to deposit sufficient energy in a small zone. This is planned to be achieved by the collision of the plasma sheaths of two or more coaxial plasma accelerators (CPA). As a primary step a single accelerator has been investigated with 2% hydrogen in helium gas mixture. Its results will be compared to the upcoming collision to learn more about the physics of plasma collision. Contrary to the gas puff valve setup of the Marshall-type in the presented experiment the recipient is prefilled with gas. Thus it is similar to a plasma focus device. However in comparison to plasma focus devices inner and outer electrode have the same length and a solid inner electrode to hinder the plasma to deposit energy into a pinch. In section II experimental setup and working principal will be described in more detail.

II. Experimental Setup and Working Principle

A. Working Principle

The presented plasma accelerator is show in Fig. 1. It is built up of an inner electrode connected to high voltage and a grounded outer electrode. The electrodes are made of stainless steel and arranged in coaxial configuration with an L-shaped insulator in between made of PEEK. The inner electrode has a diameter of 9 mm, the outer electrode is 14 mm in diameter, respectively, so the gap between the electrodes is 2.5 mm. After applying a sufficient voltage to the inner electrode the electric field causes the ignition of a discharge near the insulator. Under the achieved conditions the acceleration of the plasma

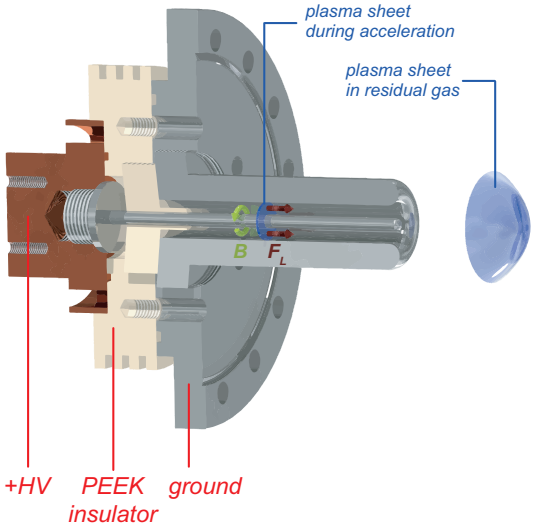

Fig. 1. Working principle and electrode setup

* Sponsored by the BMBF

can be described by the snowplow model [11]. It describes the plasma as an infinite thin sheet, which is accelerated by the resulting Lorentz force due to the radial current flow and the induced azimuthal magnetic field around the inner electrode which works like a magnetic piston. The high sheet velocity results in a shock wave that ionizes the residual gas that then becomes part of the plasma sheet. After leaving the area in between of the electrodes the plasma velocity decreases due to interaction with the residual gas until the sheet is stopped and the particles have recombined.

B. Experimental Setup and Diagnostics

A CAD model of the experimental setup with the most important components and diagnostics are depicted in Fig. 2. The capacitors with a total capacitance of $C = 27\,\mu F$ are charged by a high voltage power supply to maximum voltages of $U = 10\,kV$. The device is switched by a thyratron. Hence it can be used above self-breakdown voltage (Paschen-like). The stored energy of up to $E = 1.35kJ$ flows through a transmission line to the inner electrode and leads to maximum currents of about $I = 147kA$. Due to the low total inductance of the setup of $L = 130\,nH$ a frequency of about $f = 86kHz$ and current rise rates in the 10^{11} A/s range are achieved, which are necessary for the validity of the snowplow model [12].

C. Diagnostics

The diagnostics are placed in a 6-way vacuum vessel where the plasma is accelerated into (see Fig. 2). For the characterization of the plasma accelerator several diagnostics have been used which are listed in the following:

1) Voltage: The used voltage probe (1000:1) has an accuracy of 6% and is applied at the high voltage side of the capacitors.

2) Current: The measurement of current is performed by the use of a Rogowski coil with a systematical error of 1.5%. It is placed around the transmission line in between of capacitors and inner electrode.

3) Gas Pressure Gauges: For gas pressure estimation a species independent capacitive manometer is with a high accuracy of 0.2% of reading is used.

4) Plasma Sheet Dynamics Velocity: For plasma sheet velocity and visualization of the shape two different methods are utilized:

a) Camera: The used ICCD camera allows exposure times down to 2 ns for capturing the plasma shape. From the difference of location and time of pictures taken at different times the velocity can be calculated. This method needs several discharges at the same parameters which slightly differ from each other. Images have been performed side-on and end-on.

b) Diode Array: To simplify velocity measurement an array of 6 photodiodes in the direction of propagation is installed. This allows us to measure average velocities in between the diodes at only a single discharge.

5) Kinetic Energy: To determine the kinetic energy of the plasma cloud a length adjustable piezoelectric element is used. It is not calibrated so that the results are only qualitative. For the intended application this is sufficient. The piezo element is encased to hinder the plasma to influence its measurements.

6) Spectroscopy: To investigate electron density and temperature a 0.5 m spectrograph with a resolution down to 0.031 nm is used. The optical fiber can be installed either side-on or end-on.

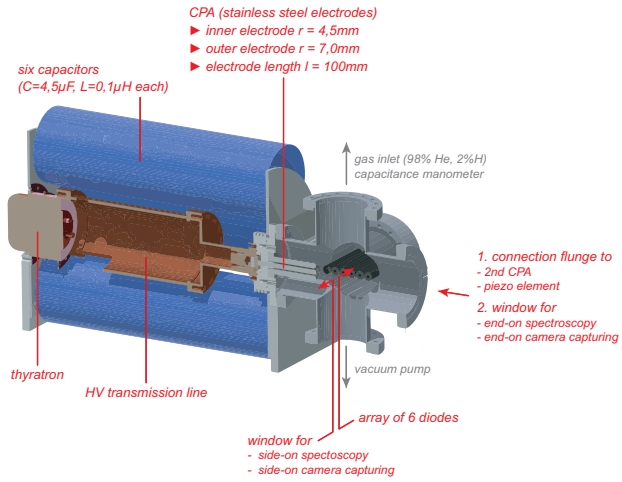

Fig. 2 Experimental setup and diagnostics

III. Experimental Results

In this section the experimental results of plasma sheet velocity, kinetic energy measurements, electron density and temperature will be presented. At pressures below 3 mbar no plasma sheet is formed, but only a diffuse discharge. So the investigations focus on a pressure range above 3 mbar.

A. Current and Voltage Characteristics

The typical behavior of current and voltage are presented in Fig. 3. An applied voltage of 9 kV leads to peak currents of approximately 120 kA. The pulse forming network consisting of capacitance, inductance and ohmic resistance leads to LCR circuit-like electrical characteristics. Due to the movement of the plasma sheet, the total inductance increases until the plasma leaves the space between the electrodes. The slight

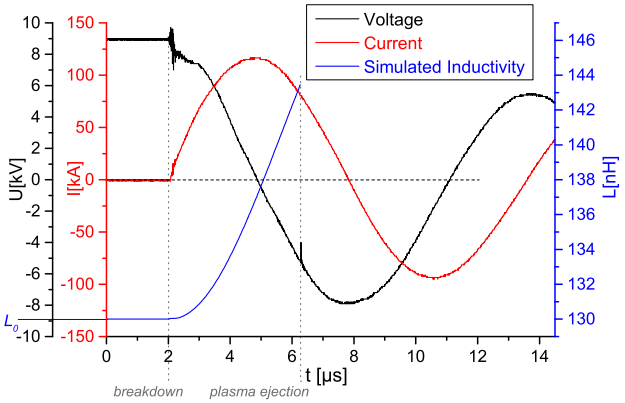

Fig. 3. Exemplary current and voltage characteristics at a discharge voltage of 9 kV

inductance increase of 13.4 nH until outlet of the first plasma sheet has been simulated and is depicted in Fig. 3 as well. After ejection a new plasma sheet ignites near the insulator. The energy loss leads to a slow decay of current and voltage.

B. Plasma Sheet Velocity

The photodiode array allows to investigate the time evolution of the plasma outside the electrodes at six places at intervals of 17 mm. For the estimation of the plasma velocity at the end of the electrodes the five measured average velocities have extrapolated to $z = 0$. To reduce influence of the statistical diversity of the shots, every measurement has been repeated ten times. The values in Fig. 4 show the averaged experimental results in black color and the simulated velocities in blue. The error bars of the velocity show the statistical deviations. For simulations the 2.5D-snow plow model [11] has been used. As can be seen in the Fig. 4, simulation and experiment fit well at lower voltages. But at higher voltages, especially at lower pressures, the experimental velocities are significantly lower than simulated. It is assumed that this is caused by the limited current-carrying capacity of the helium gas so that part of the current is carried by the much heavier electrode material. This assumption is corroborated by spectroscopic investigations. They show a higher line intensity ratio of iron to helium at lower pressures and higher voltages.

C. Plasma Propagation

The plasma propagation and shape have been investigated by taking pictures with a PI-MAX 2 ICCD camera operating in a wavelength range from 180 - 900 nm, which is limited by the used BK7-window transmission to 300 - 900 nm. The camera has a minimum exposure time of 2 ns and a resolution of 1024x1024 pixels. Exemplary results of the plasma propagation at $p = 15$ mbar and $U = 9$ kV are presented in Fig. 5 (end-on view) and Fig. 6 (side-on view) in false-color. The exposure time of the side-on captures is 100 ns and of the end-on 20 ns, respectively. $t = 0$ is set as the trigger time of the thyratron. Because of the delay of the thyratron the plasma starts to ignite after about 2.5 µs. Then, the plasma fills the whole ring and starts to get accelerated. At approximately $t = 4.5$ µs the plasma sheet starts to leave the space between the electrodes and interacts with the residual gas in the discharge vessel, leading to a deceleration.

D. Kinetic Plasma Energy

To estimate the force of the plasma sheet in dependency on the breakdown voltage a piezoelectric element is used. Its working principle is based on the direct piezoelectric effect: By the application of a force on the piezo element the generated voltage is measured with the oscilloscope with a time resolution in nanosecond scale. It is placed in 18 mm distance to the end of the electrodes and has a circular area with a diameter of 19 mm. That consequences that only the central part of the plasma sheet is detected, which is most interesting for the upcoming collision. For the determination of the plasma kinetic energy the piezo power U^2/R has been time-integrated with $R = 50\,\Omega$, as exemplarily shown in Fig. 7. To make sure that the peak of the first plasma sheet is analyzed, the diode signal is considered. The piezo element is not calibrated so the

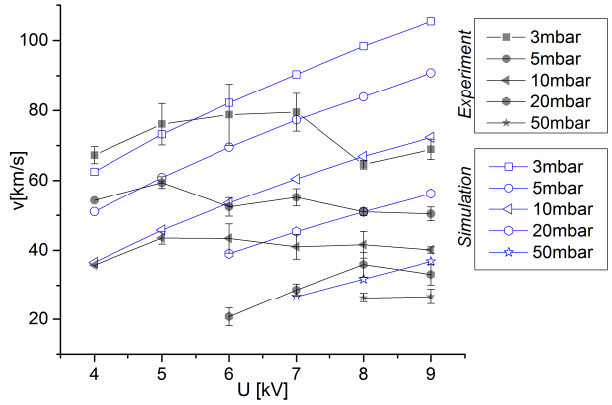

Fig. 4. Velocity measurements and simulation results at different pressures

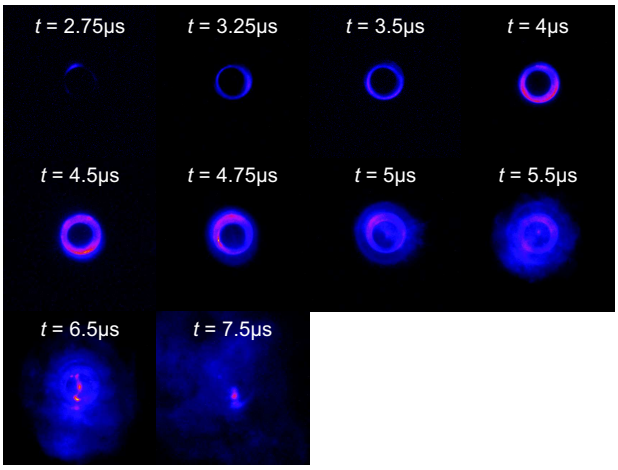

Fig. 5. End-on captures of the plasma sheet at 15 mbar and 9 kV

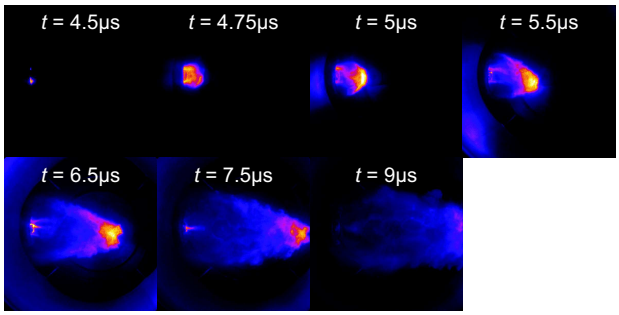

Fig. 6. Side-on captures of the plasma sheet at 15 mbar and 9 kV

results of the plasma energy presented in Fig. 8 are only qualitative. Each data point shows the average value of ten shots, whose deviation is depicted by the error bars. As can be seen in Fig. 8, the maximum kinetic energy range is approximately at ambient pressures between <5 mbar at 5 kV, 3-15 mbar at 7 kV and 5-20 mbar at 9 kV, respectively. The curves shape is explainable by following: In the lower pressure regime the sheet velocity is much higher, but the accelerated particle number is lower. In contrast, at higher pressures the accelerated mass is higher, but the velocity is significantly lower.

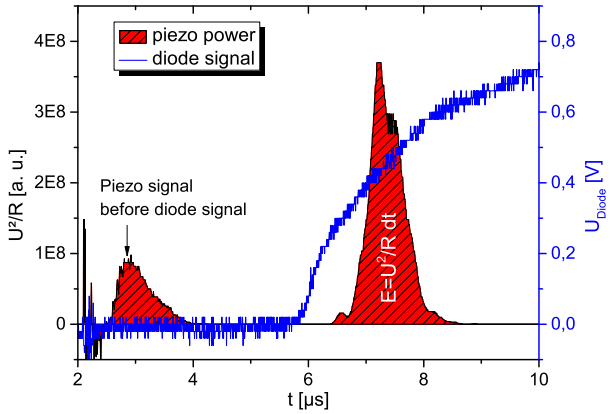

Fig. 7. Exemplary analysis of a piezo signal at 10 mbar and 9 kV

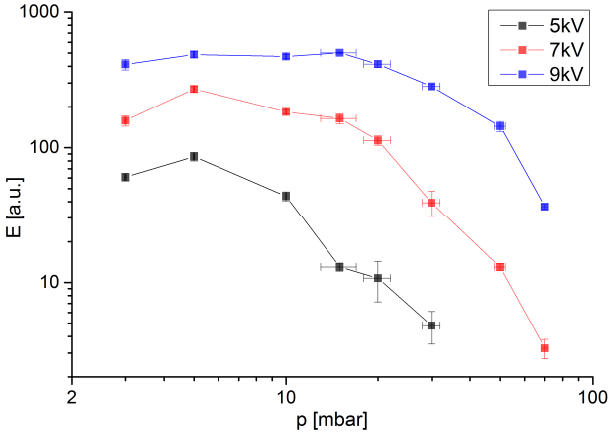

Fig. 8. Qualitative results of kinetic energy measurements by a piezoelectric element

E. Electron Density

The estimation of electron density has been performed with time and spatial integrated measurements of the Stark broadening of the H_β-line. The electron density has been deduced by the formula of Fleurier, which is valid from 10^{13} cm^{-3} to 10^{17} cm^{-3} with an accuracy of 10% [13]. For the H_β-line it is given by

$$n_e = 1.03 \cdot 10^{16} \cdot \Delta\lambda_{1/2}{}^{1.488}\,[\mathrm{cm}^{-3}] \qquad (1)$$

where $\Delta\lambda_{1/2}$ is the Lorentzian full width of half maximum of the line in nanometers. The advantage of this semi-empirical formula is the independence on density range and electron temperature. Gaussian broadening due to Doppler effect and spectrometer have been estimated and withdrawn. Again the measurements have been repeated ten times for each parameter. The analyzed results are presented in Fig. 9 and show a voltage-dependent maximum of up to approximately $n_e = 6.5 \cdot 10^{15}$ cm^{-3} at $U = 9$ kV. The electron density peak corresponds to the parameters where the plasma ejection time is equal to the time of the first current zero crossing. Due to the unequal plasma velocities at different parameters the ejection

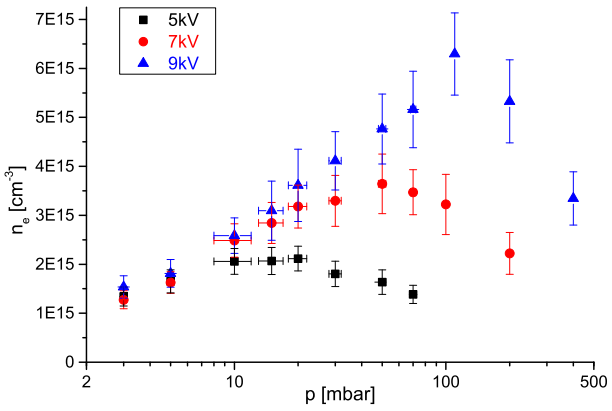

Fig. 9. Electron density at discarge voltages of 5 kV, 7 kV and 9 kV

time differs as well. This explains the shift of the maximum electron densities to lower pressures.

F. Temperature

To estimate the temperature of the discharge He I-line (471.31 nm) and He II-line (468.57 nm) intensities have been integrated and compared. With the assumption of a LTE or a PLTE for lines of different charge states the electron temperature can be calculated by the combination of equations (2) and (3):

$$\frac{I'Ag\lambda'}{IA'g'\lambda} = \mathrm{y}(\Delta E) \qquad (2)$$

$$\mathrm{y}(\Delta E) = \ln\left[\frac{1}{4\pi a_0^3 n_e}\left(\frac{kT_e}{E_\mathrm{H}}\right)^{3/2}\right] - \frac{1}{kT_e}\cdot\Delta E \qquad (3)$$

where I is the integrated line intensity, $A \cdot g$ the transition propability, λ the wavelength, a_0 the Bohr radius, kT_e the electron temperature, E_H the ionization energy of hydrogen and ΔE the energy gap including ionization energy of the used line species [14]. The parameters of the higher ionized lines are marked by the prime symbol. Due to the high energy gap between different ionization states this method is more precise than the classical Boltzmann plot with the same number of analyzed spectral lines.

The calculated temperatures are in the range of 0.7 eV to 0.8 eV. The spectroscopic measurements are time and optical path length integrated. Using FLYCHK (http://nlte.nist.gov/FLY/) to calculate a helium charge state distribution at the measured electron densities in the 10^{15} cm^{-3} to 10^{16} cm^{-3} range the simulations show a proportion of He II only at temperatures above 1.6 eV. This concludes that the maximum electron temperature is clearly above the measured average temperature.

IV. Conclusion and Outlook

For the single CPA velocity, kinetic energy, electron density and electron temperature have been sufficiently determined. In comparison to earlier measurements with argon

the reached velocities are about a factor of 3-4 higher and the electron densities are in the same range [15]. These investigations hold promising results for the collision of two or more plasma sheets. Furthermore the optimal parameter range for high kinetic energy, electron density and electrode length have been determined.

ACKNOWLEDGMENT

The authors would like to thank "Bundesministerium für Forschung und Bildung" (BMBF) and "Deutscher Akademischer Austauschdienst" (DAAD) for their support.

REFERENCES

[1] J. Marshall, "Acceleration of plasma into vacuum", Proc. 2nd United Nations Conf. on the Peaceful Uses of Atomic Energy, vol. 31, pp. 341–347, 1958.

[2] J. W. Mather, "Formation of a high-density deuterium plasma focus", Phys. Fluids, vol. 8, no. 2, pp. 366–377, 1965.

[3] P. F. Little, and B. E. Avis, "Performance of a coaxial plasma gun", J. Nucl. Energy, Part C, vol. 8, no.1, p. 11, 1965.

[4] J. Ziemer, and E. Choueiri "Dimensionless performance model for gas-fed pulsed plasma thrusters", 34th Joint Propulsion Conf., Cleveland, OH, 1998.

[5] D. Willenborg, and C. Hendricks, "Design and construction of a dense plasma focus device", Charged Particle Research Lab., Univ. Illinois, Champaign, Final Rep. Part I, 1976.

[6] E. Bogolyubov, V. D. Bochkov, V. A. Veretennikov, L. T. Vekhoreva, V. A. Gribkov, A. V. Dubrovskii, Y. P. Ivanov, A. I. Isakov, O. N. Krokhin, and P. Lee, "A powerful soft X-ray source for X-ray lithography based on plasma focusing", Phys. Scripta, vol. 57, pp. 488–494, 1998.

[7] F. Witherspoon, A. Case, S. J. Messer, R. Bomgardner, M. W. Phillips, S. Brockington, and R. Elton, "A contoured gap coaxial plasma gun with injected plasma armature", Rev. Sci. Instrum., vol. 80, no. 2, p. 83506, 2009.

[8] D. Cheng, "Application of a deflagration plasma gun as a space propulsion thruster", AIAA J., vol. 9, no. 9, pp. 1681–1685, 1971.

[9] M. Iberler, K. Esser, A. Fedjuschenko, C. Hock, J. Jacoby, B. Koubeck, B. Klump, B. J. Lee, J. Otto, M. Pfaff, T. Rienecker, and A. Schönlein, "Optical and electrical investigations of a high power Lorentz drift based gas discharge switch", IEEE 35th Int. Conf. on Plasma Science, Karlsruhe, Germany, p. 1, 2008.

[10] V. Shevelko, Private communication, 2015.

[11] M. Frignani, "Simulation of gas breakdown and plasma dynamics in plasma focus devices", Ph.D. dissertation, Univ. Bologna, Bologna, Italy, 2007.

[12] R. G. Jahn, "Physics of electric propulsion", New York: McGraw-Hill, 1968.

[13] C. Fleurier, A. Sanba, D. Hong, J. Mathias, and J. C. Pellcier, "Plasma diagnostics in the heavy ion beam-dense plasma interaction experiment at orsay", J. Phys., vol. 49, pp. 141–149, 1988.

[14] H. R. Griem, "Principles of plasma spectroscopy", New York: McGraw-Hill, 1964.

[15] J. Wiechula, C. Hock, M. Iberler, T. Manegold, A. Schönlein, and J. Jacoby, "Experimental characterization of a coaxial plasma accelerator for a colliding plasma experiment", Phys. Plasmas, vol. 22, p. 43516, 2015.